


Critical temperature of the nonadiabatic superconducting state in mono- and bilayer systemsK. A. Krok,¹ M. M. Adamczyk,² A. P. Durajski³ ,³ and R. Szcześniak^{2,3,*}¹*Ulica Gen. J. Rómmla 6/9, 42-100 Kłobuck, Poland*²*Department of Theoretical Physics, Jan Długosz University in Częstochowa, Avenue Armii Krajowej 13/15, 42-200 Częstochowa, Poland*³*Department of Physics, Częstochowa University of Technology, Avenue Armii Krajowej 19, 42-200 Częstochowa, Poland*

(Received 6 April 2023; revised 28 June 2023; accepted 3 August 2023; published 15 August 2023)

The electron-phonon interaction can induce the superconducting state in the low-dimensional mono- and bilayer systems. However, the calculated value of the temperature of the transition from the metallic to the superconducting state is greatly affected by the accuracy of the applied model. If taken into account, the vertex corrections to the electron-phonon interaction are usually of significant value due to the low Fermi level of such materials and were found to contribute to the reduction of the calculated value of the critical temperature of the transition. This fact weakens the prospects for the possibility of induction of the nonadiabatic superconducting state at the relatively high critical temperature since an increase either in the electron-phonon coupling constant or in the Debye frequency leads to the simultaneous increase in the corrected Migdal ratio, while influencing the critical temperature to a greater degree.

DOI: [10.1103/PhysRevB.108.054512](https://doi.org/10.1103/PhysRevB.108.054512)**I. INTRODUCTION**

Two-dimensional (2D) materials have garnered significant attention in current scientific research due to their exceptional physical properties, making them highly promising for applications in modern technology [1,2]. Among the most notable representatives of this category, we find graphene [3], silicene [4–8], borophene [9–11], stanene [12], plumbene [13–15], phosphorene [16–18], and others. Another class of materials that is extensively investigated is the transition metal dichalcogenides (TMDCs), such as molybdenum disulfide (MoS₂) [19–21]. In their monolayer form, TMDC materials exhibit semiconductor behavior, making them suitable for applications in optoelectronics, spintronics, flexible electronics, valleytronics, energy harvesting, and the biosensor field.

It is noteworthy that the exceptional properties of the aforementioned materials are predominantly observed in their low-dimensional forms [22,23]. A prime exemplar of such a two-dimensional system is graphene, which was first mechanically isolated from graphite in 2004 [3]. Graphene exhibits a particularly intriguing characteristic of remarkably high electron mobility even at room temperature, owing to its massless band structure. However, pure graphene lacks an energy gap at the Fermi level, resulting in a low on/off ratio and restricting its utility in the semiconductor industry [24].

Some other 2D materials gained particular attention owing to their potentially good superconducting properties. Systems of this type can be applied as elements of the nanodevices such as quantum interferometers or transistors [25–27]. The attention is focused especially on the materials which exhibit high values of the critical temperature: graphene (8% *p* doped) ($T_C = 108$ K) [28,29], *h*CN monolayer ($T_C = 105.6$ K) [30],

Li-graphene ($T_C = 36.7$ K) [31], and Li-*h*BN bilayer ($T_C = 31.9$ K) [32,33]. Naturally, there exists a much larger group of 2D superconductors, but they exhibit lower values of the critical temperature [34–50] (see Table I and II).

In all of the mentioned cases, the superconducting state is induced by classic electron-phonon interaction [51–53]. This observation is rather encouraging since it was demonstrated on the basis of the density functional theory (DFT) method [54,55] in which the coupling between the electronic and the phononic subsystems can generate superconducting states characterized by very high values of critical temperature, as can be seen, e.g., for H₃S ($T_C = 204$ K) [56–58], ScH₉ ($T_C = 233$ K) [59], ThH₁₀ ($T_C = 241$ K) [60], LaH₁₀ ($T_C = 288$ K) [61–63], and YH₁₀ ($T_C = 326$ K) [64]. It should be noticed that the theoretical predictions for these materials were essentially confirmed by the performed experiments: $[T_C]_{\text{H}_3\text{S}} = 150$ K, $[T_C]_{\text{H}_3\text{S}} = 203$ K [65,66], $[T_C]_{\text{ThH}_{10}} = 161$ K [67], and $[T_C]_{\text{LaH}_{10}} = 250$ –260 K [68,69].

The above-stated facts potentially support the possibility of the existence of the high-temperature superconducting state in 2D materials. Nevertheless, the 2D systems are characterized by the abnormally high value of the corrected Migdal ratio $M \equiv \lambda\omega_D/\varepsilon_F$ [70–73] (see Table I), which is of the order of 10^{-4} for the conventional low-temperature superconductors [74]. The symbol λ stands for the electron-phonon coupling constant, ε_F represents the value of the Fermi level, and ω_D denotes the Debye frequency. The precise determination of the Debye frequency in real materials poses challenges due to the potential mixing of acoustic and optical modes at arbitrary \mathbf{k} points within the Brillouin zone. In this study, we define the parameter ω_D as the upper limit of frequency at which the phonon density of states exhibits a nonzero value.

One can notice that the vertex corrections greatly influence the properties of the superconducting state for large values of M . This is evidenced by the results obtained for such bulk

*radoslaw.szczeniak@pcz.pl

TABLE I. Values of the corrected Migdal ratio M and the Migdal ratio ω_D/ε_F for selected low-dimensional mono- and bilayer materials. Additionally, the values of the electron-phonon coupling constant λ , the Debye frequency ω_D , and the Fermi level ε_F are given.

Lp	Compounds	M	ω_D/ε_F	λ	ω_D (meV)	ε_F (meV)
1	Li- <i>h</i> BN bilayer [32]	0.464	0.396	1.17	166	418
2	Black phosphorene (4% tensile biaxial strain) [34]	0.412	0.258	1.6	47	183
3	Graphane (8% <i>p</i> doped) [28]	0.259	0.180	1.44	174	969
4	β_0 - <i>h</i> PC monolayer [35]	0.212	0.144	1.48	157	1097
5	Li-MoS ₂ bilayer [36] <i>h</i> CN monolayer [30]	0.169	0.18	0.94	52	290
6	(40% <i>p</i> doped, 15.6% tensile biaxial strain)	0.137	0.041	3.35	133	3251
7	Ca- <i>h</i> BN monolayer [37]	0.118	0.08	1.45	181	2260
8	Li-blue phosphorene bilayer [38]	0.105	0.088	1.2	52	717
9	Li-graphene bilayer [39]	0.099	0.115	0.86	182	1577
10	Silicene (5% tensile biaxial strain) [40]	0.099	0.095	1.04	63	667
11	Li-graphene (on a <i>h</i> BN substrate) [41]	0.09	0.134	0.67	182	1353
12	Li-graphene (10% tensile biaxial strain) [31]	0.089	0.122	0.73	132	1804
13	Li-graphene monolayer [42]	0.088	0.145	0.61	193	1333
14	Na-blue phosphorene bilayer [38]	0.082	0.075	1.1	51	686
15	Sr- <i>h</i> BN monolayer [37]	0.062	0.088	0.71	177	2017
16	Black phosphorene 1 electron/cell doped [43]	0.059	0.055	1.08	62	1128
17	Ba- <i>h</i> BN monolayer [37]	0.054	0.095	0.57	178	1876
18	Li-black phosphorene bilayer [44]	0.048	0.041	1.16	58	1410
19	Mg-blue phosphorene bilayer [38]	0.032	0.04	0.8	51	1284
20	Borophene β_{12} [45]	0.027	0.03	0.89	151	5013
21	Borophene χ_3 [45]	0.027	0.028	0.95	158	5656

systems as cuprates [75–77], fullerene compounds [78,79], and heavy fermion systems [80], and for the 3D materials under high magnetic fields [81].

The presented work proves that calculations including the vertex corrections give lower values of the critical temperature of the transition into the superconducting state than those resulting from the “classic” solution, as far as the 2D materials specified in Table I are concerned. The value of T_C can be correctly calculated by means of the system of equations derived by Freericks *et al.* [82] (the vertex corrections (VC) model). This system is mathematically more complicated than the classic Migdal-Eliashberg (ME) equations [70,83,84]. It means that the self-consistent calculations made to find the critical temperature are much more difficult and time consuming. Therefore, after performing calculations for several representative systems, we found a regression formula, which

gives a good approximation of the actual value of the critical temperature if its value, calculated while neglecting the non-adiabatic effects (i.e., according to either the ME model or the Allen-Dynes formula [85]), is known.

II. ISOTROPIC FREERICKS EQUATIONS INCLUDING THE VERTEX CORRECTIONS

The equations describing the superconducting state which take into account the vertex corrections with accuracy up to the fourth order with respect to the electron-phonon coupling function g were derived by Freericks *et al.* and published in their report [82]. Originally, these equations were applied for the analysis of the influence of vertex corrections on the thermodynamic properties of the superconducting state induced in lead. The equations have the form

$$\varphi_n = \pi k_B T \sum_{m=-N}^N \frac{\lambda_{n,m} - \mu_m^*}{\sqrt{\omega_m^2 Z_m^2 + \varphi_m^2}} \varphi_m - A \frac{\pi^3 (k_B T)^2}{4\varepsilon_F} \sum_{m=-N}^M \sum_{m'=-N}^N \frac{\lambda_{n,m} \lambda_{n,m'}}{\sqrt{(\omega_m^2 Z_m^2 + \varphi_m^2)(\omega_{m'}^2 Z_{m'}^2 + \varphi_{m'}^2)(\omega_{-n+m+m'}^2 Z_{-n+m+m'}^2 + \varphi_{-n+m+m'}^2)}} \times [\varphi_m \varphi_{m'} \varphi_{-n+m+m'} + 2\varphi_m \omega_{m'} Z_{m'} \omega_{-n+m+m'} Z_{-n+m+m'} - \omega_m Z_m \omega_{m'} Z_{m'} \varphi_{-n+m+m'}] \quad (1)$$

and

$$Z_n = 1 + \frac{\pi k_B T}{\omega_n} \sum_{m=-N}^N \frac{\lambda_{n,m}}{\sqrt{\omega_m^2 Z_m^2 + \varphi_m^2}} \omega_m Z_m - A \frac{\pi^3 (k_B T)^2}{4\varepsilon_F \omega_n} \sum_{m=-N}^N \sum_{m'=-N}^N \frac{\lambda_{n,m} \lambda_{n,m'}}{\sqrt{(\omega_m^2 Z_m^2 + \varphi_m^2)(\omega_{m'}^2 Z_{m'}^2 + \varphi_{m'}^2)(\omega_{-n+m+m'}^2 Z_{-n+m+m'}^2 + \varphi_{-n+m+m'}^2)}} \times [\omega_m Z_m \omega_{m'} Z_{m'} \omega_{-n+m+m'} Z_{-n+m+m'} + 2\omega_m Z_m \varphi_{m'} \varphi_{-n+m+m'} - \varphi_m \varphi_{m'} \omega_{-n+m+m'} Z_{-n+m+m'}]. \quad (2)$$

TABLE II. Values of the critical temperature for selected materials calculated according to various methods: critical temperature T_C^{ME} obtained for the Migdal-Eliashberg model (either directly from the Eliashberg equations or by means of the Allen-Dynes formula) (the first data column); critical temperature calculated numerically including the influence of vertex corrections (the second data column); critical temperature calculated from the formula (4) including the influence of vertex corrections (the third data column).

Lp	Compounds	T_C^{ME} (K)	T_C^{VC} (K) numerically	T_C^{VC} (K) acc. to formula (4)
1	Li- <i>h</i> BN bilayer	31.9 ^a [33]	19.1 [33]	19
2	Black phosphorene (4% tensile biaxial strain)	19.7 ^a	11.9	12.6
3	Graphene (8% <i>p</i> doped)	108 ^a [29]	78.4	83.6
4	β_0 - <i>h</i> PC monolayer	17.1 ^a	14.1	13.9
5	Li-MoS ₂ bilayer <i>h</i> CN monolayer	10.5 ^a	9.3	9
6	(40% <i>p</i> doped, 15.6% tensile biaxial strain)	105.6 ^a	79.6 [87]	93
7	Ca- <i>h</i> BN monolayer	12.8 ^b	11.2	10.9
8	Li-blue phosphorene bilayer	23.5 ^a	19.5	21.4
9	Li-graphene bilayer	14.7 ^a [48]	13.7	13.4
10	Silicene (5% tensile biaxial strain)	18.7 ^a [47]	16.3	17.1
11	Li-graphene (on a <i>h</i> BN substrate)	13 ^b	12.4	12
12	Li-graphene (10% tensile biaxial strain)	36.7 ^a	34.6	33.8
13	Li-graphene monolayer	6.2 ^a [50]	5.8 [50]	5.7
14	Na-blue phosphorene bilayer	20.1 ^b	19.1	18.7
15	Sr- <i>h</i> BN monolayer Black phosphorene	5.8 ^b	5.7	5.5
16	1 electron/cell doped	10.8 ^a	10.2	10.2
17	Ba- <i>h</i> BN monolayer	1.5 ^b	1.48	1.5
18	Li-black phosphorene bilayer	16.5 ^b	15.7	15.8
19	Mg-blue phosphorene bilayer	14.4 ^b	14	14
20	Borophene β_{12}	18.7 ^b	18.5	18.3
21	Borophene χ_3	24.7 ^b	24.2	24.1

^aMigdal-Eliashberg

^bAllen-Dynes

The symbol $\varphi_n = \varphi(i\omega_n)$ denotes the function of the order parameter, and $Z_n = Z(i\omega_n)$ is the wave-function renormalization factor. The fermionic Matsubara frequency is given by the formula $\omega_n = \pi k_B T (2n + 1)$, N stands for the number of the Matsubara frequencies, and k_B is the Boltzmann constant. The order parameter is defined by the ratio $\Delta_n = \varphi_n / Z_n$. The isotropic pairing kernel for the electron-phonon interaction has the form

$$\lambda_{n,m} = 2 \int_0^{\omega_D} d\omega \frac{\omega}{\omega^2 + 4\pi^2 (k_B T)^2 (n-m)^2} \alpha^2 F(\omega), \quad (3)$$

where $\alpha^2 F(\omega)$ is the spectral function of the electron-phonon interaction (the so-called Eliashberg function). The depairing electronic correlations are modeled by means of the expression $\mu_n^* = \mu^* \theta(\omega_c - |\omega_n|)$, where θ represents the Heaviside function and ω_c is the cutoff frequency ($\omega_c = 3\omega_D$).

The equations proposed by Freericks *et al.* allow one to determine the values of both the order parameter and the wave-function renormalization factor in the self-consistent manner. Therefore, the results obtained by means of them can be sensibly compared with results calculated with use of the classic Migdal-Eliashberg model ($A = 0$).

The equations proposed by Freericks *et al.* were solved for the purpose of the present work for a large number of Matsubara frequencies ($N = 4000$), which allowed one to obtain the

stable solutions for φ_n and Z_n within the temperature range $T_0 \sim 2-3$ K to the critical temperature. Numerical methods described in another publication [86] of ours were applied to solve the equations presented above.

III. THE INFLUENCE OF VERTEX CORRECTIONS ON THE VALUE OF CRITICAL TEMPERATURE

Twenty-one representative 2D systems were selected in such a way that the range of the corrected Migdal ratio values would be as wide as possible. They were fully analyzed according both to the Migdal-Eliashberg equations and the equation proposed by Freericks *et al.* It should be mentioned here that the full results with respect to the thermodynamic properties of the Li-graphene monolayer, as well as of the Li-*h*BN bilayer, were already published by members of our team elsewhere [33,50].

The obtained results prove that considerations that take into account the vertex corrections lead to the decreased values of the critical temperature. The values of T_C calculated within both the ME and the VC models are juxtaposed in Table II. Considering these sets of data, we noticed that the decrease of critical temperature was larger the greater was the value of the corrected Migdal ratio. This tendency is shown in Fig. 1, in which the dependence between the relative change of the

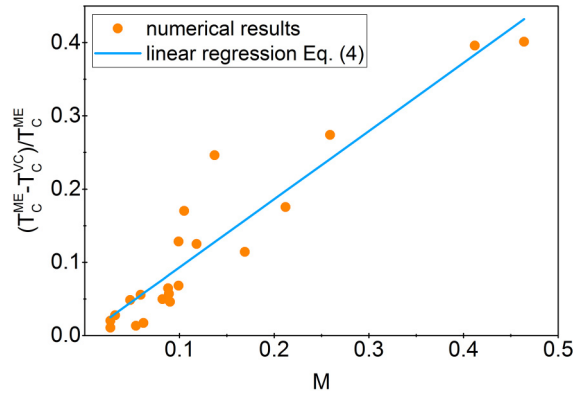


FIG. 1. The dependence of the relative difference between the values of critical temperatures T_C^{ME} and T_C^{VC} on the corrected Migdal ratio M . The value of $\mu^* = 0.1$ was assumed for all systems, excluding LiC_6 . The value of $\mu^* = 0.114$ for LiC_6 was found from the available experimental data [50]. The blue line corresponds to Eq. (4).

value of critical temperature, $(T_C^{\text{ME}} - T_C^{\text{VC}})/T_C^{\text{ME}}$, and the ratio M is presented. This system of coordinates allows one to find an equation of linear regression (represented by the blue line in the diagram),

$$\frac{T_C^{\text{ME}} - T_C^{\text{VC}}}{T_C^{\text{ME}}} = 0.931M. \quad (4)$$

The corrected coefficient of determination for formula (4) is equal to 0.942 and the standard error of estimate is 0.05.

Formula (4) is rather important from a practical point of view because it allows for easy and relatively accurate estimation of the value of critical temperature T_C^{VC} , if the values of T_C^{ME} and M are known. If the value of the Coulomb pseudopotential is low ($\mu^* \sim 0.1$), the temperature T_C^{ME} can be calculated from the Allen-Dynes formula [85]. It should be remembered, however, that this formula cannot be applied for higher values of the Coulomb pseudopotential ($\mu^* \sim 0.2$) since it significantly underestimates the value of the critical temperature in comparison to the value calculated by means of the isotropic Migdal-Eliashberg equations [88].

Formula (4) was used to calculate the realistic values of the critical temperature, i.e., the values taking into account (however indirectly) the influence of vertex corrections, for all systems presented in Table I. The results are presented both in Fig. 2 and in Table II. The magnitude of the drop in the values of the critical temperature due to the nonadiabatic effects falls within the range from 0.5% T_C^{ME} to over 40% T_C^{ME} . It is worth paying particular attention to the materials characterized by high values of the critical temperature, i.e., graphane (8% p doped), $h\text{CN}$ monolayer, $\text{Li-}h\text{BN}$, and phosphorene (strain 8%). For all the mentioned cases, high values of T_C^{ME} result from the high values of the electron-phonon coupling constants (exceeding 1 in every case). Therefore, even the not-so-large value of the ω_D/ε_F ratio does not significantly restrict the high value of the corrected Migdal ratio ($\lambda\omega_D/\varepsilon_F$). As a consequence, one should expect a relevant decrease in the value of the critical temperature after taking into account

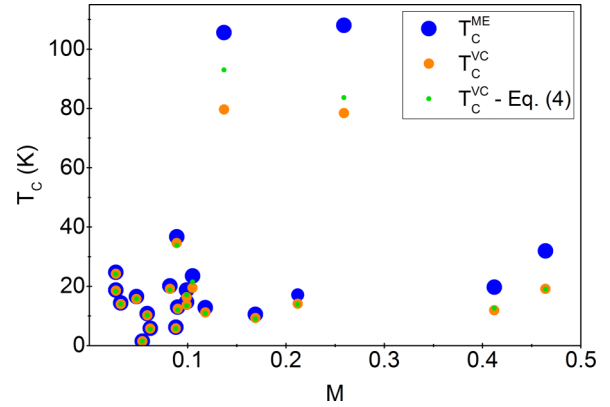


FIG. 2. The dependence of the critical temperature on the corrected Migdal ratio M for materials characterized in Tables I and II.

the vertex corrections in the model. Actually, this fact can be easily noticed in Fig. 2.

One more mechanism which could potentially yield the high value of the critical temperature is worth discussing. Let us introduce the formula based on the BCS theory [89,90]: $k_B T_C = 1.13\omega_D \exp(-1/\lambda)$. The formula states that the critical temperature will rise with an increase in the Debye frequency. Unfortunately, the ω_D/ε_F ratio grows in this case as well. Even if the intermediate value of the electron-phonon coupling constant is assumed (e.g., ~ 0.6), which is the most optimistic option, one still cannot expect the desirable reduction of the corrected Migdal ratio. The situation described above occurs, for example, in the case of a LiC_6 superconductor, for which $\omega_D = 193$ meV and $\lambda = 0.61$ [42]. All things considered, a conclusion can be drawn that the 2D systems in which the superconducting state can be induced exhibit such small values of the Fermi level that one cannot neglect the influence of the vertex corrections to the electron-phonon interaction, and this effect contributes to the decrease in the calculated value of the critical temperature. As a consequence, the possible increase in the critical temperature due to the increased λ or ω_D will be strongly restricted by the simultaneous increase in the corrected Migdal ratio.

It is worth noting the limitations of Eq. (4) and its potential application for analyzing 3D systems. In the first step, let us observe that the first constraint on the value of parameter M is related to the linear form of the discussed expression and the condition that both T_C^{ME} and T_C^{VC} are greater than or equal to zero. A straightforward analysis allows us to obtain a possible value for parameter M , which ranges from 0 to 1.074.

In our opinion, there is an additional constraint associated with the perturbative nature of the Freericks *et al.* equations, which suggests caution when applying Eq. (4) to superconductors characterized by an electron-phonon coupling constant greater than one and very high values of T_C^{ME} , around 100 K. This conclusion is supported by the results gathered in Table II, where it can be observed that for the graphane systems (8% p doped) and $h\text{CN}$ monolayer, the differences between the T_C^{VC} and $[T_C]_{\text{Eq. (4)}}$ values are approximately 6.6% and 14.4%, respectively.

Furthermore, let us note that the analysis presented in this section is based on the Migdal-Eliashberg equations and

the equation proposed by Freericks *et al.*, which have identical forms for both 2D and 3D systems (the dimensional information of the studied system is only contained in the Eliashberg function). Therefore, Eq. (4) can also be applied to three-dimensional systems. For example, in the case of lead, we have $T_C^{\text{ME}} = 7.23$ K [82] and $T_C^{\text{VC}} = 7.175$ K [91], resulting in $(T_C^{\text{ME}} - T_C^{\text{VC}})/T_C^{\text{ME}} = 0.0076$. On the other hand, for $M = 7.8 \times 10^{-3}$ [92], we obtain $0.931M = 0.0073$. The agreement between the results is therefore very good. However, for the superconductor K_3C_{60} ($[T_C^{\text{ME}}]_{\mu^*=0.1} = 59.1$ K and $T_C^{\text{VC}} = 19.5$ K [93]), due to the excessively high value of the parameter $M = 1.473$ [71,93], we expect our model to break down, as confirmed by the following estimation: $(T_C^{\text{ME}} - T_C^{\text{VC}})/T_C^{\text{ME}} = 0.67$ and $0.931M = 1.371$.

IV. ANISOTROPY OF THE PAIRING KERNEL VERSUS THE VALUE OF THE CRITICAL TEMPERATURE: A CASE OF LiC_6

The results discussed in the previous section were obtained for the isotropic approximation (solutions of the thermodynamic equations did not explicitly depend on the wave vector \mathbf{k}). Now the question was if including the dependence on \mathbf{k} in the model would significantly change the previously obtained results. Please notice that to answer it, one should solve the thermodynamical equations that are dependent both on the Matsubara frequency and on the wave vector in the self-consistent manner. Unfortunately, the numerical complexity of such an approach was too high. Nevertheless, a partial insight into the considered problem was achieved by analyzing the values of the anisotropic kernel of the electron-phonon interaction ($K_{\mathbf{k}\mathbf{q}\mathbf{q}_1\mathbf{q}_2}^{(4)}$). The negative values of the kernel would indicate the weakened electron-phonon pairing, also pointing to an even further drop of the critical temperature for this model. Similarly, the positive values of the $K_{\mathbf{k}\mathbf{q}\mathbf{q}_1\mathbf{q}_2}^{(4)}$ would be responsible for an increase in the T_C values.

Derivation of the formula for the anisotropic pairing kernel consisted in putting the Migdal-Eliashberg approximation aside and calculating the required thermodynamic Green functions via successive iterations of the equations of motion [94–96]. The procedure began with the definition of a matrix function,

$$\begin{aligned} G_{\mathbf{k}}(i\omega_n) &= \langle\langle \Psi_{\mathbf{k}} | \Psi_{\mathbf{k}}^\dagger \rangle\rangle_{i\omega_n} \\ &= \begin{pmatrix} \langle\langle c_{\mathbf{k}\uparrow} | c_{\mathbf{k}\uparrow}^\dagger \rangle\rangle_{i\omega_n} & \langle\langle c_{\mathbf{k}\uparrow} | c_{-\mathbf{k}\downarrow} \rangle\rangle_{i\omega_n} \\ \langle\langle c_{-\mathbf{k}\downarrow}^\dagger | c_{\mathbf{k}\uparrow}^\dagger \rangle\rangle_{i\omega_n} & \langle\langle c_{-\mathbf{k}\downarrow}^\dagger | c_{-\mathbf{k}\downarrow} \rangle\rangle_{i\omega_n} \end{pmatrix}, \end{aligned} \quad (5)$$

where $\Psi_{\mathbf{k}} = (c_{\mathbf{k}\uparrow}^\dagger, c_{-\mathbf{k}\downarrow})$ denotes the Nambu spinor, and $\Psi_{\mathbf{k}}^\dagger$ stands for its Hermitian coupling. The symbol $c_{\mathbf{k}\sigma}$ ($c_{\mathbf{k}\sigma}^\dagger$) is the operator of annihilation (creation) of the electronic state of momentum \mathbf{k} and spin $\sigma \in \{\uparrow, \downarrow\}$. Please notice that above the critical temperature, the diagonal elements $G_{\mathbf{k}}(i\omega_n)$ describe properties of the metallic state, while below the T_C , all elements of the matrix express the thermodynamics of the superconducting condensate, whereas the antidiagonal elements are related to the average number of Cooper pairs.

The formalism was based on the Fröchlich Hamiltonian [53], which models the linear coupling between the electronic and the phononic systems,

$$\begin{aligned} H &= \sum_{\mathbf{k}\sigma} \bar{\varepsilon}_{\mathbf{k}} \Psi_{\mathbf{k}}^\dagger \tau_3 \Psi_{\mathbf{k}} + \sum_{\mathbf{q}} \omega_{\mathbf{q}} b_{\mathbf{q}}^\dagger b_{\mathbf{q}} \\ &+ \frac{1}{\sqrt{N}} \sum_{\mathbf{k}\mathbf{q}\sigma} g_{\mathbf{q}} \Psi_{\mathbf{k}+\mathbf{q}}^\dagger \tau_3 \Psi_{\mathbf{k}} \phi_{\mathbf{q}}, \end{aligned} \quad (6)$$

where $\bar{\varepsilon}_{\mathbf{k}} = \varepsilon_{\mathbf{k}} - \mu$, $\varepsilon_{\mathbf{k}}$ is the band energy of electrons, and μ stands for the chemical potential. Function $\omega_{\mathbf{q}}$ represents the phonon dispersion relation. The symbol $b_{\mathbf{q}}$ ($b_{\mathbf{q}}^\dagger$) denotes the annihilation/creation operator for the phononic state of momentum \mathbf{q} . Furthermore, $\phi_{\mathbf{q}} = b_{-\mathbf{q}}^\dagger + b_{\mathbf{q}}$, and the τ_3 quantity is a diagonal Pauli matrix.

The algorithm applied to calculate $K_{\mathbf{k}\mathbf{q}\mathbf{q}_1\mathbf{q}_2}^{(4)}$ is presented in Fig. 3, complemented with the algorithm for deriving the classic Migdal-Eliashberg equations for the purpose of comparison. After doing the required calculations, we arrived at

$$\begin{aligned} K_{\mathbf{k}\mathbf{q}\mathbf{q}_1\mathbf{q}_2}^{(4)} &= -g_{\mathbf{q}} g_{-\mathbf{q}-\mathbf{q}_1-\mathbf{q}_2} g_{\mathbf{q}_1} g_{\mathbf{q}_2} \frac{\tanh \frac{\bar{\varepsilon}_{\mathbf{k}-\mathbf{q}-\mathbf{q}_1}}{2k_B T_C}}{\bar{\varepsilon}_{\mathbf{k}-\mathbf{q}-\mathbf{q}_1}} \\ &\times \frac{(\pi k_B T_C)^2 + \bar{\varepsilon}_{\mathbf{k}-\mathbf{q}} \bar{\varepsilon}_{\mathbf{k}-\mathbf{q}-\mathbf{q}_1-\mathbf{q}_2}}{[(\pi k_B T_C)^2 + \bar{\varepsilon}_{\mathbf{k}-\mathbf{q}}^2][(\pi k_B T_C)^2 + \bar{\varepsilon}_{\mathbf{k}-\mathbf{q}-\mathbf{q}_1-\mathbf{q}_2}^2]} \\ &\times \frac{\text{ctgh}\left(\frac{\omega_{\mathbf{q}}}{2k_B T_C}\right) \delta_{\mathbf{q}_1, -\mathbf{q}_2} + \text{ctgh}\left(\frac{\omega_{\mathbf{q}_1}}{2k_B T_C}\right) \delta_{\mathbf{q}_1, -\mathbf{q}_2}}{(\omega_{\mathbf{q}} + \omega_{\mathbf{q}_1})}. \end{aligned} \quad (7)$$

While analyzing the formula (7), one can notice that the phonon dispersion relation cannot change the value of the kernel $K_{\mathbf{k}\mathbf{q}\mathbf{q}_1\mathbf{q}_2}^{(4)}$ from a negative to positive one because the $\omega_{\mathbf{q}}$ function never is negative.

We assumed that the electron-phonon matrix elements have the structure predicted by Bloch [97,98]: $g_{\mathbf{q}} = g_0 |\mathbf{q}| / \sqrt{\omega_{\mathbf{q}}}$. However, close to the Fermi level, it is also possible to apply the model proposed by Perali *et al.* [99], $g_{\mathbf{q}} = \sqrt{\gamma(q_c)/q_c^2 + \omega_{\mathbf{q}}^2}$, where q_c denotes the momentum cutoff. The $g_{\mathbf{q}}$ function cannot change the sign of the pairing kernel value in either case. The sign of the kernel value can be changed only if the following inequality is true: $(\pi k_B T_C)^2 + \bar{\varepsilon}_{\mathbf{k}-\mathbf{q}} \bar{\varepsilon}_{\mathbf{k}-\mathbf{q}-\mathbf{q}_1-\mathbf{q}_2} < 0$. Due to the momentum conservation principle, only two momentum channels are open: $\mathbf{q}_1 = -\mathbf{q}_2$ and $\mathbf{q} = -\mathbf{q}_2$. The first channel does not lead to the change of sign of the negative kernel value because $\bar{\varepsilon}_{\mathbf{k}-\mathbf{q}} \bar{\varepsilon}_{\mathbf{k}-\mathbf{q}-\mathbf{q}_1-\mathbf{q}_2} \rightarrow \bar{\varepsilon}_{\mathbf{k}-\mathbf{q}}^2 > 0$. The sign of the $K_{\mathbf{k}\mathbf{q}\mathbf{q}_1\mathbf{q}_2}^{(4)}$ function can be changed only in the $\mathbf{q} = -\mathbf{q}_2$ channel. Hence, one can conclude that the $K_{\mathbf{k}\mathbf{q}\mathbf{q}_1\mathbf{q}_2}^{(4)}$ kernel is depairing as long as the following condition is fulfilled:

$$v \equiv (\pi k_B T_C)^2 + \bar{\varepsilon}_{\mathbf{k}+\mathbf{q}_2} \bar{\varepsilon}_{\mathbf{k}-\mathbf{q}_1} > 0. \quad (8)$$

A further thorough discussion of this condition was possible only for an actual example of a physical system. We selected the LiC_6 compound ($T_C \sim 5.9$ K [100]), which is well worth consideration due to the significant value of the corrected Migdal ratio ($M \sim 0.09$) and the availability of both experimental and theoretical results of its examination.

The scheme of an LiC_6 crystal structure is presented in Fig. 4. Gray lines represent the hexagonal lattice with carbon

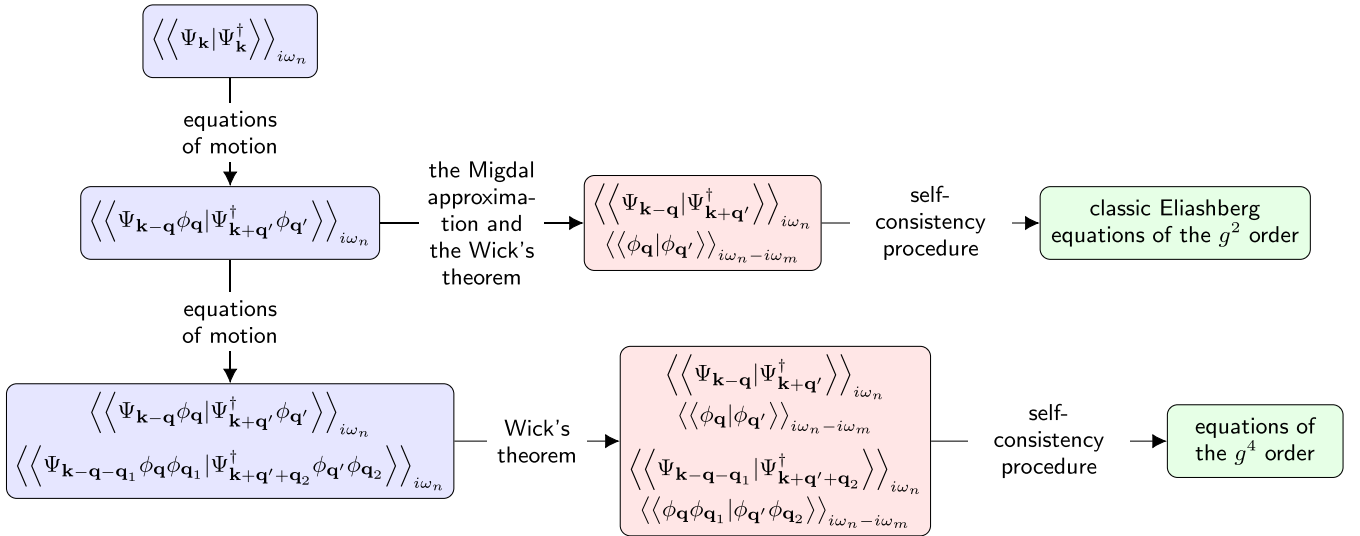


FIG. 3. Block diagram of the derivation of the thermodynamic equations of the second (g^2) and the fourth (g^4) order. The straightforward and full presentation of classic Migdal-Eliashberg equations can be found in [84].

atoms located at the nodes. Green lines mark the effective triangular lattice determined by the lithium atoms (s -type dopant).

Results of the calculations with respect to the electronic and the phononic dispersion relations for the LiC_6 compound obtained according to the DFT method are available in the professional literature [42]. We came to the respective results by means of the effective triangular lattice (ETL) model. In this model, the electronic dispersion relation takes the form

$$\bar{\epsilon}_{\mathbf{k}} = -2t \left[\cos(k_x) + 2 \cos\left(\frac{k_x}{2}\right) \cos\left(\frac{\sqrt{3}}{2}k_y\right) \right] - \mu, \quad (9)$$

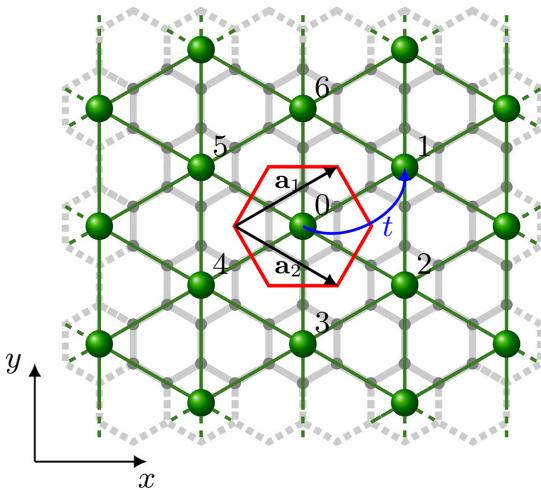


FIG. 4. Effective triangular lattice of the LiC_6 compound. Large green dots denote lithium atoms; small green-gray dots are carbon atoms. A unit cell of the triangular lattice is marked in red, its central atom is denoted as “0,” and the nearest neighbors are numbered consecutively. The \mathbf{a}_1 and \mathbf{a}_2 black arrows represent the lattice translation vectors, $\mathbf{a}_1 = [\frac{\sqrt{3}}{2}, \frac{1}{2}]$, $\mathbf{a}_2 = [\frac{\sqrt{3}}{2}, -\frac{1}{2}]$. The blue arrow schematically marks the hopping of the electron characterized by the hopping integral t .

where the lattice constant is taken as unity. The phononic dispersion relation can be expressed by the formula

$$\omega_{\mathbf{q}} = \omega_0 \sqrt{3 - \cos(q_x) - 2 \cos\left(\frac{q_x}{2}\right) \cos\left(\frac{\sqrt{3}}{2}q_y\right)}. \quad (10)$$

We obtained the following estimation of the initial parameters of the model: $t = 355$ meV and $\omega_0 = 13.3$ meV, which in the units of the hopping integral gives $\omega_0 = 0.0375 t$. The effective value of the g_0 amplitude of the electron-phonon interaction is equal to $0.00543t$. A graphic representation of the results obtained either by means of the DFT method or from the ETL model can be found in Fig. 5. Further details regarding the ETL model can be found in the Appendix A.

Then we proceeded to a detailed analysis of the condition (8) for the considered compound. To do this, we first took into account 10^7 randomly selected vectors \mathbf{k} , \mathbf{q}_1 , and \mathbf{q}_2 belonging to the first Brillouin zone and found the corresponding values of the ν parameter. Figure 6 presents the character (the sign) of the resulting values of ν as a function of the length of both the \mathbf{q}_1 and \mathbf{q}_2 vectors. It can instantly be seen that the condition (8) is not fulfilled for many sets of \mathbf{k} , \mathbf{q}_1 , and \mathbf{q}_2 vectors. This means that the kernel $K_{\mathbf{k}\mathbf{q}\mathbf{q}_1\mathbf{q}_2}^{(4)}$ can also be the pairing one in the momentum channel $\mathbf{q} = -\mathbf{q}_2$. Nevertheless, the decisive factor is the magnitude of the $K_{\mathbf{k}\mathbf{q}\mathbf{q}_1\mathbf{q}_2}^{(4)}$ function values for both the pairing and the depairing cases. So the second step consisted in performing further calculations, which eventually proved that the average kernel value for the totally depairing channel $\mathbf{q}_1 = -\mathbf{q}_2$ was equal to $-0.00603t^2$, while for the $\mathbf{q} = -\mathbf{q}_2$ channel, it was equal to $-3.24467 \times 10^{-6}t^2$ (so it also indicated depairing). Similarly, the result was found to be $-0.11455t^2$ for both momentum channels being active ($\mathbf{q} = \mathbf{q}_1$).

The presented analysis allows one to conclude that for the case of the LiC_6 superconductor, taking into account the

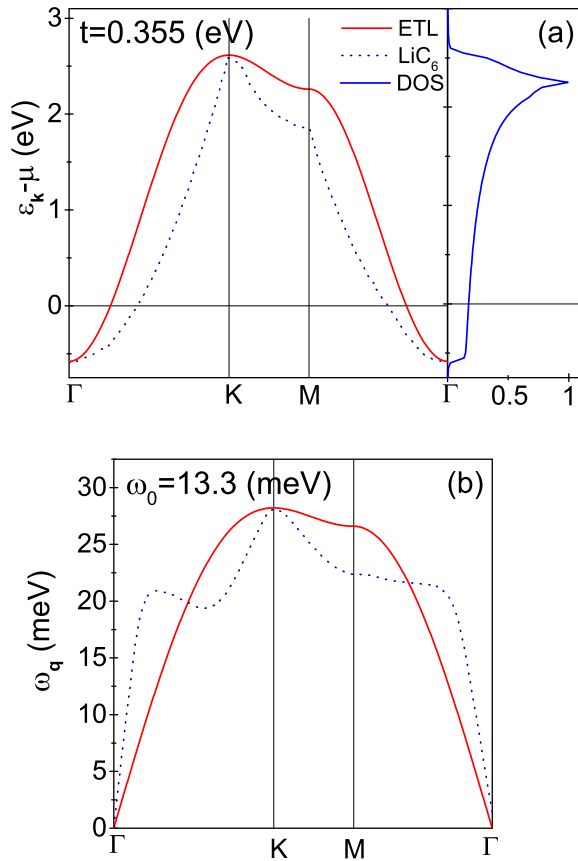


FIG. 5. Data for LiC_6 compound. (a) The electronic band near the Fermi level. (b) Phononic dispersion relation. Blue dotted lines correspond to the results obtained by the DFT method [42]. Red solid lines illustrate the results obtained for the ETL model.

vertex corrections which explicitly include the momentum transition does not lead to the increase in the critical temperature with respect to the T_C^{VC} value.

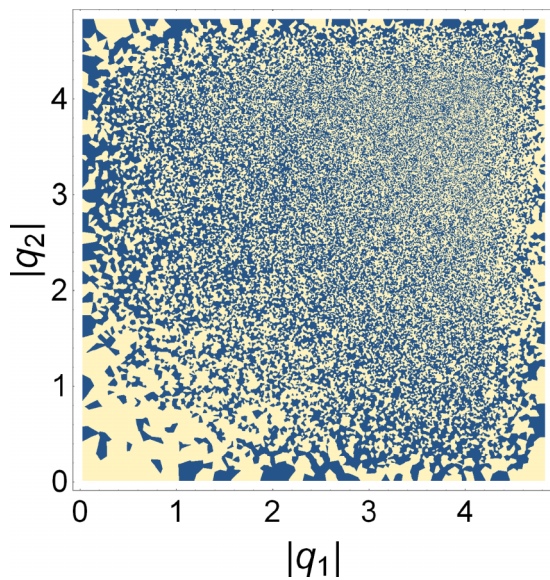


FIG. 6. The dependence of sign of the ν parameter value on the length of the \mathbf{q}_1 and \mathbf{q}_2 vectors. The blue areas correspond to the negative values; the yellow areas indicate the positive ones.

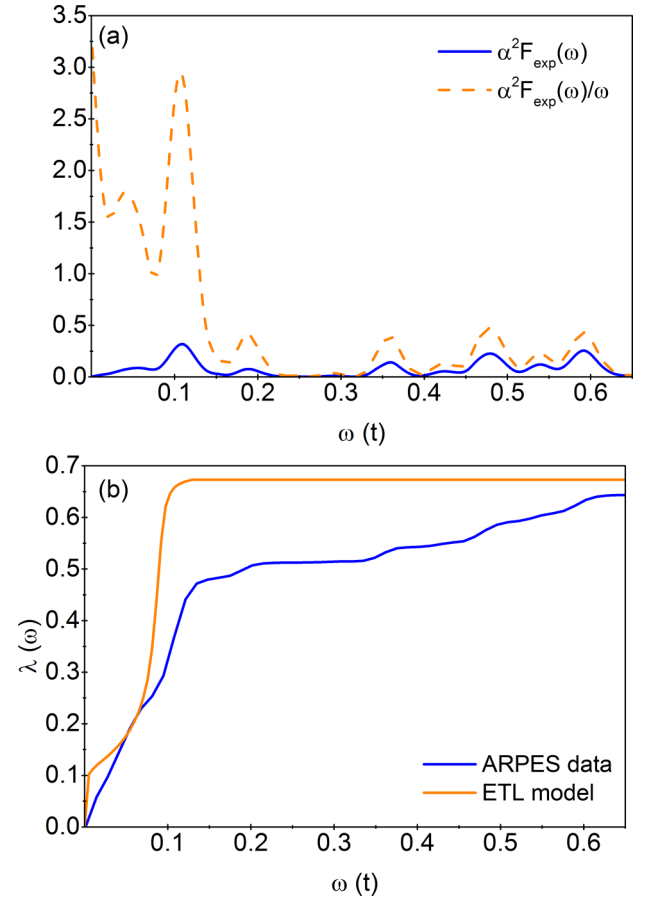


FIG. 7. (a) The experimental Eliashberg function for the LiC_6 superconductor, obtained through the use of the ARPES method [100], provides valuable insight into the dominant contribution to the electron-phonon coupling function, as expressed by the ratio $\alpha^2 F_{\text{exp}}(\omega)/\omega$. (b) The electron-phonon coupling function, determined based on experimental data [100] and in the framework of the effective triangular lattice model.

Although the tedious calculations were performed only for the LiC_6 compound, it should be emphasized that the applied procedure can be used in a similar way for any other physical system of interest, but the final result will not necessarily be the same.

V. CONCLUSION

The 2D compounds analyzed during the study are characterized by significantly higher values of the corrected Migdal ratio than the conventional low-temperature superconductors. Therefore, taking into account the vertex corrections to the electron-phonon interaction while determining the thermodynamical properties of these compounds decreases the calculated value of the critical temperature as compared to the one found with the use of the classic Migdal-Eliashberg equations. The critical temperature of the phase transition from the metallic to the superconducting state for the considered group of materials always takes the value lower than 100 K.

It is worth emphasizing that there exists a simple dependence between the values of the critical temperature determined either with or without taking into account the

vertex corrections. Namely, the relative change in the value of the critical temperature due to the introduction of the vertex corrections, $(T_C^{\text{ME}} - T_C^{\text{VC}})/T_C^{\text{ME}}$, is well approximated by the product of the corrected Migdal ratio M and the factor 0.931. The dependence is quite useful since it allows for easy estimation of the actual value of T_C if the critical temperature determined by means of Migdal-Eliashberg equations is known.

The predictions we presented above are based on the calculations performed within the isotropic Eliashberg-type formalism, taking into account the vertex corrections of the order of g^4 [82]. This approach has its limitations, consisting in neglecting the dependence of the pairing kernel from either the electronic or the phononic wave vector, as well as ignoring the vertex corrections of the order higher than the fourth. The significance of the omitted elements of the theory is very difficult to assess in general. Nevertheless, we proved for the LiC_6 compound that taking into account anisotropy of the pairing kernel does not lead to the increase in the value of the critical temperature. It should also be mentioned that such an increase is also not observed if the vertex correction of the sixth order is included, what was proved elsewhere [33] for the example of the $\text{Li-}h\text{BN}$ superconductor.

APPENDIX: VALIDATION OF THE ETL MODEL IN THE CONTEXT OF EXPERIMENTAL DATA FOR THE LiC_6 COMPOUND

From an experimental standpoint, the investigation of the superconducting state in alkali-doped graphene presents significant challenges. The preparation of samples is intricate and their sensitivity to external conditions further complicates the analysis. Consequently, reliable experimental data in the literature is limited. In the case of the LiC_6 compound, it is advisable to refer to [100], where the use of angle-resolved

photoemission spectroscopy (ARPES) revealed the substantial modification of the graphene phonon density of states due to lithium doping, resulting in an enhanced electron-phonon coupling. Moreover, the authors of [100] explicitly highlighted that the charge transfer from Li electrons to the graphene π^* bands is approximately 0.14 electrons per Li atom. This specific charge transfer is crucial for the formation of the Li band at the Γ point, which has been identified as a key factor in the amplification of the electron-phonon coupling [42,101,102].

The Eliashberg function, denoted as $\alpha^2 F_{\text{exp}}(\omega)$ and obtained in [100], is presented in Fig. 7(a). The complex electron and phonon structure of the LiC_6 compound is evident in the intricate shape of $\alpha^2 F_{\text{exp}}(\omega)$. However, by analyzing the frequency dependence of the electron-phonon coupling function, given by $\lambda_{\text{exp}}(\omega) = 2 \int_0^\omega d\omega' \alpha^2 F_{\text{exp}}(\omega')/\omega'$, it can be deduced that the ratio $\alpha^2 F_{\text{exp}}(\omega)/\omega$ plays a crucial role in determining the properties of the superconducting state. Based on the analysis of the function $\alpha^2 F_{\text{exp}}(\omega)/\omega$ [see Fig. 7(a)], it is evident that the electron-phonon coupling function is primarily influenced by frequencies in the range of 0 to $0.2t$. In light of this observation, the effective triangular lattice (ETL) model incorporates only this dominant contribution, effectively capturing the essential features. Consequently, a relatively good agreement is achieved between the experimentally derived electron-phonon coupling function, denoted as $\lambda_{\text{exp}}(\omega)$, and its counterpart from the ETL model, denoted as $\lambda_{\text{ETL}}(\omega)$ [see Fig. 7(b)].

Furthermore, it is worth noting that the electron-phonon coupling constant and the critical temperature obtained in [100] yield the following values: $[\lambda]_{\text{exp}} = 0.644$ and $[T_C]_{\text{exp}} = 5.9$ K, respectively. Remarkably, these experimental values align favorably with the results obtained within the framework of the effective triangular lattice model, $[\lambda]_{\text{ETL}} = 0.673$ and $[T_C]_{\text{ETL}} = 5.93$ K, as determined using the Allen-Dynes formula [85].

-
- [1] Y. Chen, Z. Fan, Z. Zhang, W. Niu, C. Li, N. Yang, B. Chen, and H. Zhang, Two-dimensional metal nanomaterials: Synthesis, properties, and applications, *Chem. Rev.* **118**, 6409 (2018).
- [2] B. Liu and K. Zhou, Recent progress on graphene-analogous 2D nanomaterials: Properties, modeling and applications, *Prog. Mater. Sci.* **100**, 99 (2019).
- [3] K. S. Novoselov, A. K. Geim, S. V. Morozov, D. Jiang, Y. Zhang, S. V. Dubonos, I. V. Grigorieva, and A. A. Firsov, Electric field effect in atomically thin carbon films, *Science* **306**, 666 (2004).
- [4] K. Takeda and K. Shiraishi, Theoretical possibility of stage corrugation in Si and Ge analogs of graphite, *Phys. Rev. B* **50**, 14916 (1994).
- [5] G. G. Guzmán-Verri and L. C. Lew Yan Voon, Electronic structure of silicon-based nanostructures, *Phys. Rev. B* **76**, 075131 (2007).
- [6] S. Cahangirov, M. Topsakal, E. Akturk, H. Sahin, and S. Ciraci, Two- and One-Dimensional Honeycomb Structures of Silicon and Germanium, *Phys. Rev. Lett.* **102**, 236804 (2009).
- [7] B. Aufray, A. Kara, S. B. Vizzini, H. Oughaddou, C. LeAndri, B. Ealet, and G. L. Lay, Graphene-like silicon nanoribbons on Ag(110): A possible formation of silicene, *Appl. Phys. Lett.* **96**, 183102 (2010).
- [8] B. Lalmi, H. Oughaddou, H. Enriquez, A. Kara, S. B. Vizzini, B. N. Ealet, and B. Aufray, Epitaxial growth of a silicene sheet, *Appl. Phys. Lett.* **97**, 223109 (2010).
- [9] I. Boustani, New quasi-planar surfaces of bare boron, *Surf. Sci.* **370**, 355 (1997).
- [10] A. J. Mannix, X. F. Zhou, B. Kiraly, J. D. Wood, D. Alducin, B. D. Myers, X. Liu, B. L. Fisher, U. Santiago, J. R. Guest, M. J. Yacaman, A. Ponce, A. R. Oganov, M. C. Hersam, and N. P. Guisinger, Synthesis of borophenes: Anisotropic, two-dimensional boron polymorphs, *Science* **350**, 1513 (2015).
- [11] B. Feng, J. Zhang, Q. Zhong, W. Li, S. Li, H. Li, P. Cheng, S. Meng, L. Chen, and K. Wu, Experimental realization of two-dimensional boron sheets, *Nat. Chem.* **8**, 563 (2016).
- [12] J. C. Garcia, D. B. de Lima, L. V. C. Assali, and J. F. Justo, Group IV graphene and graphane-like nanosheets, *J. Phys. Chem. C* **115**, 13242 (2011).
- [13] D. K. Das, J. Sarkar, and S. K. Singh, Effect of sample size, temperature and strain velocity on mechanical properties of plumbene by tensile loading along longitudinal direction:

- A molecular dynamics study, *Comput. Mater. Sci.* **151**, 196 (2018).
- [14] H. Zhao, L. Ping, B. Zhang, S. Yan, L. Sheng, R. Zhang, W. Ji, S. Yan, and Z. C. Shishen, Unexpected giant-gap quantum spin Hall insulator in chemically decorated plumbene monolayer, *Sci. Rep.* **6**, 20152 (2016).
- [15] L. Zhang, H. Zhao, W. Ji, C. Zhang, P. Li, and P. Wang, Discovery of a new quantum spin hall phase in bilayer plumbene, *Chem. Phys. Lett.* **712**, 78 (2018).
- [16] H. Liu, A. T. Neal, Z. Zhu, Z. Luo, X. Xu, D. Tomanek, and P. D. Ye, Phosphorene: An unexplored 2D semiconductor with a high hole mobility, *ACS Nano* **8**, 4033 (2014).
- [17] L. Li, Y. Yu, Y. Jun, G. Guo, Q. Ge, X. Ou, H. Wu, and Y. Zhang, Black phosphorus field effect transistors, *Nat. Nanotechnol.* **9**, 372 (2014).
- [18] S. P. Koenig, R. A. Doganov, A. H. Castro-Neto, and B. Ozyilmaz, Electric field effect in ultrathin black phosphorus, *Appl. Phys. Lett.* **104**, 103106 (2014).
- [19] A. Splendiani, L. Sun, Y. Zhang, T. Li, J. Kim, C. Y. Chim, G. Galli, and F. Wang, Emerging photoluminescence in monolayer mos_2 , *Nano Lett.* **10**, 1271 (2010).
- [20] B. Radisavljevic, A. Radenovic, J. Brivio, V. Giacometti, and A. Kis, Emerging photoluminescence in monolayer MoS_2 , *Nat. Nanotechnol.* **6**, 147 (2011).
- [21] A. Eftekhari, Tungsten dichalcogenides (WS_2 , WSe_2 , and WTe_2): Materials chemistry and applications, *J. Mater. Chem. A* **5**, 18299 (2017).
- [22] P. Miró, M. Audiffred, and T. Heine, An atlas of two-dimensional materials, *Chem. Soc. Rev.* **43**, 6537 (2014).
- [23] H. Tian, J. Tice, R. Fei, V. Tran, X. Yan, L. Yang, and H. Wang, Low-symmetry two-dimensional materials for electronic and photonic applications, *Nano Today* **11**, 763 (2016).
- [24] A. H. Castro Neto, F. Guinea, N. M. R. Peres, K. S. Novoselov, and A. K. Geim, The electronic properties of graphene, *Rev. Mod. Phys.* **81**, 109 (2009).
- [25] J. Delahaye, J. Hassel, R. Lindell, M. Sillanpää, M. Paalanen, H. Seppä, and P. Hakonen, Low-noise current amplifier based on mesoscopic Josephson junction, *Science* **299**, 1045 (2003).
- [26] S. D. Franceschi, L. Kouwenhoven, C. Schönenberger, and W. Wernsdorfer, Hybrid superconductor quantum dot devices, *Nat. Nanotechnol.* **5**, 703 (2010).
- [27] O.-P. Saira, M. Meschke, F. Giazotto, A. M. Savin, M. Mtnen, and J. P. Pekola, Heat Transistor: Demonstration of Gate-Controlled Electronic Refrigeration, *Phys. Rev. Lett.* **99**, 027203 (2007).
- [28] G. Savini, A. C. Ferrari, and F. Giustino, First-Principles Prediction of Doped Graphane as a High-Temperature Electron-Phonon Superconductor, *Phys. Rev. Lett.* **105**, 037002 (2010).
- [29] A. P. Durajski, Influence of hole doping on the superconducting state in graphane, *Supercond. Sci. Technol.* **28**, 035002 (2015).
- [30] J. Zhou, Q. Sun, Q. Wang, and P. Jena, High-temperature superconductivity in heavily N - or B -doped graphene, *Phys. Rev. B* **92**, 064505 (2015).
- [31] J. Pešić, R. Gajić, K. Hingerl, and M. Belić, Strain-enhanced superconductivity in Li-doped graphene, *Europhys. Lett.* **108**, 67005 (2013).
- [32] N. H. Shimada, E. Minamitani, and S. Watanabe, Theoretical prediction of phonon-mediated superconductivity with $T_C \approx 25$ k in Li-intercalated hexagonal boron nitride bilayer, *Appl. Phys. Express* **10**, 093101 (2017).
- [33] K. A. Szewczyk, I. A. Domagalska, A. P. Durajski, and R. Szcześniak, Nonadiabatic superconductivity in Li-intercalated hexagonal boron nitride bilayer, *Beilstein J. Nanotechnol.* **11**, 1178 (2020).
- [34] Y. Ge, W. Wan, F. Yang, and Y. Yao, The strain effect on superconductivity in phosphorene: A first-principles prediction, *New J. Phys.* **17**, 035008 (2015).
- [35] B. T. Wang, P. F. Liu, T. Bo, W. Yin, O. Eriksson, J. Zhao, and F. Wang, Superconductivity in two-dimensional phosphorus carbide ($\beta_0 - \text{PC}$), *Phys. Chem. Chem. Phys.* **20**, 12362 (2018).
- [36] G. Q. Huang, Z. W. Xing, and D. Y. Xing, Dynamical stability and superconductivity of Li-intercalated bilayer MoS_2 : A first-principles prediction, *Phys. Rev. B* **93**, 104511 (2016).
- [37] N. H. Shimada, E. Minamitani, and S. Watanabe, Theoretical prediction of superconductivity in monolayer H-Bn doped with alkaline-earth metals (Ca, Sr, Ba), *J. Phys.: Condens. Matter* **32**, 435002 (2020).
- [38] J. Zhang and S. Dong, Prediction of above 20 K superconductivity of blue phosphorus bilayer with metal intercalations, *2D Mater.* **3**, 035006 (2016).
- [39] D. M. Guzman, H. M. Alyahyaei, and R. A. Jishi, Superconductivity in graphene-lithium, *2D Mater.* **1**, 021005 (2014).
- [40] W. Wan, Y. Ge, F. Yang, and Y. Yao, Phonon-mediated superconductivity in silicene predicted by first-principles density functional calculations, *Europhys. Lett.* **104**, 36001 (2013).
- [41] T. P. Kaloni, A. V. Balatsky, and U. Schwingenschlögl, Substrate-enhanced superconductivity in Li-decorated graphene, *Europhys. Lett.* **104**, 47013 (2014).
- [42] G. Profeta, M. Calandra, and F. Mauri, Phonon-mediated superconductivity in graphene by lithium deposition, *Nat. Phys.* **8**, 131 (2012).
- [43] D. F. Shao, W. J. Lu, H. Y. Lv, and Y. P. Sun, Electron-doped phosphorene: A potential monolayer superconductor, *Europhys. Lett.* **108**, 67004 (2014).
- [44] G. Q. Huang, Z. W. Xing, and D. Y. Xing, Prediction of superconductivity in Li-intercalated bilayer phosphorene, *Appl. Phys. Lett.* **106**, 113107 (2015).
- [45] M. Gao, Q.-Z. Li, X.-W. Yan, and J. Wang, Prediction of phonon-mediated superconductivity in borophene, *Phys. Rev. B* **95**, 024505 (2017).
- [46] A. K. Geim and I. V. Grigorieva, Van der Waals heterostructures, *Nature (London)* **499**, 419 (2013).
- [47] A. P. Durajski, D. Szcześniak, and R. Szcześniak, Study of the superconducting phase in silicene under biaxial tensile strain, *Solid State Commun.* **200**, 17 (2014).
- [48] D. Szcześniak, Superconducting properties of lithium-decorated bilayer graphene, *Europhys. Lett.* **111**, 18003 (2015).
- [49] G. Huang and Z. Xing, Superconductivity of bilayer phosphorene under interlayer compression, *Chin. Phys. B* **25**, 027402 (2016).
- [50] D. Szcześniak and R. Szcześniak, Signatures of nonadiabatic superconductivity in lithium-decorated graphene, *Phys. Rev. B* **99**, 224512 (2019).

- [51] H. Fröhlich, Theory of the superconducting state. I. The ground state at the absolute zero of temperature, *Phys. Rev.* **79**, 845 (1950).
- [52] H. Fröhlich, Isotope effect in superconductivity, *Proc. R. Soc. London A* **63**, 778 (1950).
- [53] H. Fröhlich, Interaction of electrons with lattice vibrations, *Proc. R. Soc. London A* **215**, 291 (1952).
- [54] R. G. Parr and W. Yang, *Density-functional Theory of Atoms and Molecules* (Oxford University Press, New York, 1989).
- [55] P. Giannozzi, S. Baroni, N. Bonini, M. Calandra, R. Car, C. Cavazzoni, D. Ceresoli, G. L. Chiarotti, M. Cococcioni, I. Dabo, A. D. Corso, S. de Gironcoli, S. Fabris, G. Fratesi, R. Gebauer, U. Gerstmann, C. Gougoussis, A. Kokalj, M. Lazzeri, L. Martin-Samos *et al.*, Quantum Espresso: A modular and open-source software project for quantum simulations of materials, *J. Phys.: Condens. Matter* **21**, 395502 (2009).
- [56] D. Duan, Y. Liu, F. Tian, X. Huang, Z. Zhao, H. Yu, B. Liu, W. Tian, and T. Cui, Pressure-induced metallization of dense $(\text{H}_2\text{S})_2\text{H}_2$ with high- T_c superconductivity, *Sci. Rep.* **4**, 6968 (2014).
- [57] A. P. Durajski, R. Szcześniak, and Y. Li, Non-BCS thermodynamic properties of H_2S superconductor, *Physica C* **515**, 1 (2015).
- [58] A. P. Durajski, R. Szcześniak, and L. Pietronero, High-temperature study of superconducting hydrogen and deuterium sulfide, *Annal. Phys.* **528**, 358 (2016).
- [59] X. Ye, N. Zarifi, E. Zurek, R. Hoffmann, and N. W. Ashcroft, High hydrides of scandium under pressure: Potential superconductors, *J. Phys. Chem. C* **122**, 6298 (2018).
- [60] A. G. Kvashnin, D. V. Semenov, I. A. Kruglov, I. A. Wrona, and A. R. Oganov, High-temperature superconductivity in a Th-H system under pressure conditions, *ACS Appl. Mater. Interfaces* **10**, 43809 (2018).
- [61] F. Peng, Y. Sun, C. J. Pickard, R. J. Needs, Q. Wu, and Y. Ma, Hydrogen Clathrate Structures in Rare Earth Hydrides at High Pressures: Possible Route to Room-Temperature Superconductivity, *Phys. Rev. Lett.* **119**, 107001 (2017).
- [62] M. Kostrzewa, K. M. Szcześniak, A. P. Durajski, and R. Szcześniak, From LaH_{10} to room-temperature superconductors, *Sci. Rep.* **10**, 1592 (2020).
- [63] I. A. Kruglov, D. V. Semenov, H. Song, R. Szcześniak, I. A. Wrona, R. Akashi, M. M. Davari Esfahani, D. Duan, T. Cui, A. G. Kvashnin, and A. R. Oganov, Superconductivity of LaH_{10} and LaH_{16} polyhydrides, *Phys. Rev. B* **101**, 024508 (2020).
- [64] H. Liu, I. I. Naumov, R. Hoffmann, N. W. Ashcroft, and R. J. Hemley, Potential high- T_c superconducting lanthanum and yttrium hydrides at high pressure, *Proc. Natl. Acad. Sci. USA* **114**, 6990 (2017).
- [65] A. P. Drozdov, M. I. Eremets, and I. A. Troyan, Conventional superconductivity at 190 K at high pressures, [arXiv:1412.0460](https://arxiv.org/abs/1412.0460).
- [66] A. P. Drozdov, M. I. Eremets, I. A. Troyan, V. Ksenofontov, and S. I. Shylin, Conventional superconductivity at 203 kelvin at high pressures in the sulfur hydride system, *Nature (London)* **525**, 73 (2015).
- [67] D. V. Semenov, A. G. Kvashnin, A. G. Ivanova, V. Svitlyk, V. Y. Fomin, A. V. Sadakov, O. A. Sobolevskiy, V. M. Pudalov, I. A. Troyan, and A. R. Oganov, Superconductivity at 161 K in thorium hydride ThH_{10} : Synthesis and properties, *Mater. Today* **33**, 36 (2020).
- [68] A. P. Drozdov, P. P. Kong, V. S. Minkov, S. P. Besedin, M. A. Kuzovnikov, S. Mozaffari, L. Balicas, F. F. Balakirev, D. E. Graf, V. B. Prakapenka, E. Greenberg, D. A. Knyazev, M. Tkacz, and M. I. Eremets, Superconductivity at 250 K in lanthanum hydride under high pressures, *Nature (London)* **569**, 528 (2019).
- [69] M. Somayazulu, M. Ahart, A. K. Mishra, Z. M. Geballe, M. Baldini, Y. Meng, V. V. Struzhkin, and R. J. Hemley, Evidence for Superconductivity above 260 K in Lanthanum Superhydride at Megabar Pressures, *Phys. Rev. Lett.* **122**, 027001 (2019).
- [70] A. B. Migdal, Interaction between electrons and lattice vibrations in a normal metal, *Sov. Phys. JETP* **34**, 996 (1958).
- [71] L. Pietronero, S. Strassler, and C. Grimaldi, Nonadiabatic superconductivity. I. Vertex corrections for the electron-phonon interactions, *Phys. Rev. B* **52**, 10516 (1995).
- [72] C. Grimaldi, L. Pietronero, and S. Strassler, Nonadiabatic superconductivity. II. Generalized Eliashberg equations beyond Migdal's theorem, *Phys. Rev. B* **52**, 10530 (1995).
- [73] C. Grimaldi, L. Pietronero, and S. Strassler, Nonadiabatic Superconductivity: Electron-Phonon Interaction Beyond Migdal's Theorem, *Phys. Rev. Lett.* **75**, 1158 (1995).
- [74] P. Miller, J. K. Freericks, and E. J. Nicol, Possible experimentally observable effects of vertex corrections in superconductors, *Phys. Rev. B* **58**, 14498 (1998).
- [75] Y. J. Uemura, L. P. Le, G. M. Luke, B. J. Sternlieb, W. D. Wu, J. H. Brewer, T. M. Riseman, C. L. Seaman, M. B. Maple, M. Ishikawa, D. G. Hinks, J. D. Jorgensen, G. Saito, and H. Yamochi, Basic Similarities Among Cuprate, Bismuthate, Organic, Chevrel-Phase, and Heavy-Fermion Superconductors Shown by Penetration-Depth Measurements, *Phys. Rev. Lett.* **66**, 2665 (1991).
- [76] Y. J. Uemura, L. P. Le, G. M. Luke, B. J. Sternlieb, W. D. Wu, J. H. Brewer, T. M. Riseman, C. L. Seaman, M. B. Maple, M. Ishikawa, D. G. Hinks, J. D. Jorgensen, G. Saito, and H. Yamochi, Basic Similarities among Cuprate, Bismuthate, Organic, Chevrel-Phase, and Heavy-Fermion Superconductors Shown by Penetration-Depth Measurements, *Phys. Rev. Lett.* **68**, 2712(E) (1992).
- [77] N. d'Ambrumenil, An unconventional family tree, *Nature (London)* **352**, 472 (1991).
- [78] L. Pietronero, Superconductivity mechanism in doped C_{60} , *Europhys. Lett.* **17**, 365 (1992).
- [79] W. E. Pickett and D. M. Poirier, Electrons and phonons in C_{60} -based materials, *Solid State Phys.* **48**, 225 (1994).
- [80] R. J. Wojciechowski, Migdal's theorem in heavy fermion systems, *Phys. B* **259–261**, 498 (1999).
- [81] H. Goto and Y. Natsume, A theoretical approach to strong-coupling superconductivity in ultra-high fields in consideration of vertex corrections to Eliashberg-Migdal equations, *Phys. B: Condens. Matter* **216**, 281 (1996).
- [82] J. K. Freericks, E. J. Nicol, A. Y. Liu, and A. A. Quong, Vertex-corrected tunneling inversion in electron-phonon mediated superconductors: Pb, *Phys. Rev. B* **55**, 11651 (1997).
- [83] G. M. Eliashberg, Interactions between electrons and lattice vibrations in a superconductor, *Sov. Phys. JETP* **11**, 696 (1960).

- [84] J. P. Carbotte, Properties of boson-exchange superconductors, *Rev. Mod. Phys.* **62**, 1027 (1990).
- [85] P. B. Allen and R. C. Dynes, Transition temperature of strongly-coupled superconductors reanalyzed, *Phys. Rev. B* **12**, 905 (1975).
- [86] R. Szcześniak, The numerical solution of the imaginary-axis Eliashberg equations, *Acta Phys. Pol. A* **109**, 179 (2006).
- [87] D. Szcześniak and E. A. Drzazga-Szcześniak, Nonadiabatic superconductivity in the electron-doped graphene, *Europhys. Lett.* **135**, 67002 (2021).
- [88] R. Szcześniak and A. P. Durajski, The thermodynamic properties of the high-pressure superconducting state in the hydrogen-rich compounds, *Solid State Sci.* **25**, 45 (2013).
- [89] J. Bardeen, L. N. Cooper, and J. R. Schrieffer, Microscopic theory of superconductivity, *Phys. Rev.* **106**, 162 (1957).
- [90] J. Bardeen, L. N. Cooper, and J. R. Schrieffer, Theory of superconductivity, *Phys. Rev.* **108**, 1175 (1957).
- [91] W. B. Pearson and I. M. Templeton, Superconducting transition of lead, *Phys. Rev.* **109**, 1094 (1958).
- [92] E. F. Talantsev, Quantifying nonadiabaticity in major families of superconductors, *Nanomaterials* **13**, 71 (2023).
- [93] R. Szcześniak and A. Barasiński, Thermodynamic properties of the superconducting state in the K_3C_{60} fulleride, *Acta Phys. Pol. A* **116**, 1053 (2009).
- [94] A. L. Fetter and J. D. Walecka, *Quantum Theory of Many-Particle Systems* (McGraw-Hill Book Company, New York, 1971).
- [95] K. Elk and W. Gasser, *The Method of Green's Functions in Solid State Physics* (Akademie-Verlag, 1979).
- [96] G. Rickayzen, *Green's Functions and Condensed Matter*, 1st ed. (Academic, London, 1980).
- [97] F. Bloch, On the quantum mechanics of electrons in crystal lattices, *Z. Phys.* **52**, 555 (1928).
- [98] M. P. Allan, M. H. Fischer, O. Ostojic, and A. Andringa, Creating better superconductors by periodic nanopatterning, *SciPost Phys.* **3**, 010 (2017).
- [99] A. Perali, C. Grimaldi, and L. Pietronero, Nonadiabatic pairing effects for tight-binding electrons interacting with phonons, *Phys. Rev. B* **58**, 5736 (1998).
- [100] B. M. Ludbrook, G. Levy, P. Nigge, M. Zonno, M. Schneider, D. J. Dvorak, C. N. Veenstra, S. Zhdanovich, D. Wong, P. Dosanjh, C. Straßer, A. Stöhr, S. Forti, C. R. Ast, U. Starke, and A. Damascelli, Evidence for superconductivity in Li-decorated monolayer graphene, *Proc. Natl. Acad. Sci. USA* **112**, 11795 (2015).
- [101] M. Calandra and F. Mauri, Theoretical Explanation of Superconductivity in C_6Ca , *Phys. Rev. Lett.* **95**, 237002 (2005).
- [102] G. Csanyi, P. B. Littlewood, A. H. Nevidomskyy, C. J. Pickard, and B. D. Simons, The role of the inter-layer state in the electronic structure of superconducting graphite intercalated compounds, *Nat. Phys.* **1**, 42 (2005).